A Stiffness-Adjustable Hyperredundant Manipulator Using a Variable Neutral-Line Mechanism for Minimally Invasive Surgery

Yong-Jae Kim, Shanbao Cheng, Sangbae Kim, and Karl Iagnemma

***Abstract*—In robotic single-port surgery, it is desirable for a manipulator to exhibit the property of variable stiffness. Small-port incisions may require both high flexibility of the manipulator for safety purposes, as well as high structural stiffness for operational precision and high payload capability. This paper presents a new hyperredundant tubular manipulator with a variable neutral-line mechanisms and adjustable stiffness. A unique asymmetric arrangement of the tendons and the links realizes both articulation of the manipulator and continuous stiffness modulation. This asymmetric motion of the manipulator is compensated by a novel actuation mechanism without affecting its structural stiffness. The paper describes the basic mechanics of the variable neutral-line manipulator, and its stiffness characteristics. Simulation and experimental results verify the performance of the proposed mechanism.**

***Index Terms*—Adjustable stiffness, medical robot, snake-like manipulator, variable neutral-line mechanism.**

I. Introduction

SNAKE-like manipulators have unique characteristics and advantages such as flexibility, safety, dexterity, and potential for minimization. Most snake-like manipulators can be roughly categorized into flexible manipulators and hyperredundant manipulators. Trunk and tentacle-like devices made from soft materials belong to the flexible manipulator category [1]–[4] and they have inherent passive compliance, which is one of the great advantages of these manipulators. On the other hand, hyperredundant manipulators [5]–[7] are composed of many rigid links and joints, which can be actuated by embedded motors, as in [7], or by external actuators and transmission components such as tendons or flexible shafts [5], [6]. Most of the externally actuated hyperredundant manipulators have an underactuated property, and thus they also exhibit passive compliance like flexible manipulators.

Passive compliance is useful for the safe manipulation of unknown or delicate objects, human–robot interaction, and multiarm cooperation without complex force-feedback schemes. This compliance is caused by the flexibility of the structural material or deformable components in the mechanism. Because the compliance is determined by the material stiffness and the pose of the manipulators [2], [8], the stiffness remains fixed if the pose is determined.

Recently, snake-like manipulators are receiving high attention due to rising research interest in minimally invasive surgery (MIS) and natural orifice translumenal endoscopic surgery (NOTES) [9]–[11]. MIS and NOTES have huge advantages including low trauma, fast healing, and minimal or no scarring. Snake-like devices are well suited for accessing deep inside of the patient's abdominal cavity through a small entry point, while today's rigid (and typically straight) tools have difficultly achieving such access. However, the fixed stiffness of snake-like devices hinder their ability to achieve high stiffness for high payload operation and exact positioning and low stiffness for safe movement without harming internal organs [12], [13]. In order to overcome this drawback, various stiffening mechanisms have been developed. One popular approach relies on the use of wire tension and friction between rigid links [5], [14].

However, the wire tension must be very high, and thus the links must be strong enough to endure high tension, since the stiffening force arises solely from the friction between the links. Moreover, the links can occupy substantial space, and thus, it is difficult to create a compact manipulator that also allows a passage of miniaturized surgical tools (e.g., one with a large hollow space at the center).

Recent research has focused on the use of tunable-stiffness materials, including field-activated materials like magnetorheological or electrorheological fluids [15], [16]. These technologies are promising for the precise control of damping, and are mostly used in active damping mechanisms such as tunable automotive suspensions. However, there are limitations in their achievable range of the elastic modulus, or yield strength, when they are activated. Thermally activated materials such as wax or solder can also be used as tunable-stiffness elements to create locking mechanisms in soft robotic applications [17], [18]. However, achieving tunable stiffness with these materials requires long activation times (typically on the order of seconds).

Particle jamming technology using granular media has also recently been explored as another way to achieve tunable stiffness [19], [20]. Particle jamming has interesting features including high deformability in its fluid-like state, and drastic stiffness increase in its solid-like state, without significant change in volume, but it requires substantial volume to achieve sufficient

Manuscript received April 21, 2013; revised September 29, 2013; accepted October 12, 2013. Date of publication November 11, 2013; date of current version April 1, 2014. This paper was recommended for publication by Editor B. J. Nelson upon evaluation of the reviewers' comments. This work was supported in part by the Samsung Advanced Institute of Technology of Samsung Electronics.

Y.-J. Kim is with the Samsung Advanced Institute of Technology, Kyunggi do, Korea (e-mail: yj424.kim@samsung.com).

S. Cheng is with the Ellipse Technologies, Irvine, CA 92618 USA (e-mail: chengshanbao@gmail.com).

S. Kim and K. Iagnemma are with the Massachusetts Institute of Technology, Cambridge, MA 02139 USA (e-mail: sangbae@mit.edu; kdi@mit.edu).

Color versions of one or more of the figures in this paper are available online at http://ieeexplore.ieee.org.

Digital Object Identifier 10.1109/TRO.2013.2287975

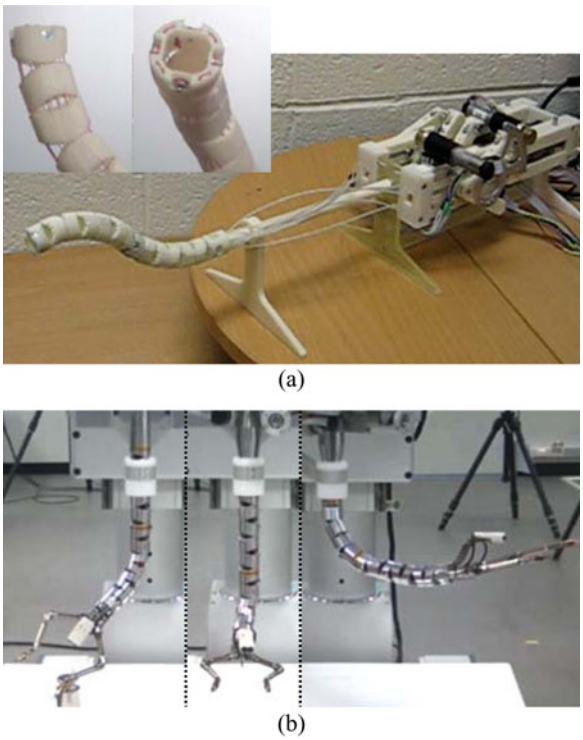

Fig. 1. (a) Four-DOF variable neutral-line manipulator and actuation system. (b) Single-port surgical system using the variable neutral-line manipulator.

stiffness. In order to overcome this problem, reduced dimensional jamming approaches, such as layer jamming of thin frictional flaps of material, have been investigated and exhibited drastic stiffness changes within a small volume [21], [22].

To overcome the drawbacks of previous methods, we propose a new snake-like mechanism, named a variable neutral-line mechanism as shown in Fig. 1, whose stiffness can be changed continuously, even while in motion. Although it is also composed of rigid links and actuated by tendons, its unique joint mechanism and actuation system make stiffness control possible by varying the tension of the tendons. Its simple, thin, and hollow structure [see the top left of Fig. 1(a)] is suitable for surgical application such as MIS or NOTES, because it can be used as a flexible guide tube through which multiple miniaturized surgical tools such as endoscopes and surgical instruments can be inserted. Fig. 1(b) shows a single-port surgical system which is composed of dual 7-degree of freedom (DOF) instruments and one 3-DOF endoscopic device mounted at the end of a guide tube made by the two identical 2-DOF variable neutral-line manipulators. To help with the rotation and insertion motion of the mounting system, the guide tube has in total 6 DOF, which means that the guide tube can place the dual instruments and the endoscope at arbitrary position in the abdominal cavity with an arbitrary approach direction. Then, the human-like configuration of the instruments and the endoscope can provide an intuitive teleoperational environment for a surgeon. Due to dexterity and adjustable stiffness of the variable neutral-line manipulator, extremely difficult surgeries using a single port (such as lower anterior resection or partial nephrectomy) can be performed significantly more easily and safely.

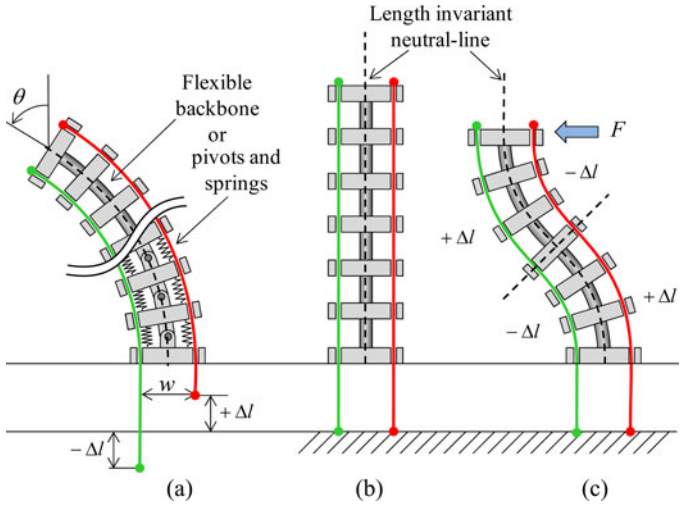

Fig. 2. One-dimensional illustration of traditional snake-like manipulators.

The paper is structured as follows. In Section II, we introduce the basic mechanics of the proposed manipulator without external forces, and then, in Section III, we exhaustively investigate the deflection shape under an external force. Based on this, Section IV derives important stiffness properties of the variable neutral-line manipulator. Section V presents an actuation system that can control both of the bending angle and the stiffness of the manipulator independently. Section VI validates the stiffness model through experiments. Section VII discusses key design parameters related to the stiffness, and suggests several useful design variations without losing the advantage of the proposed mechanism, and this is followed by the paper's conclusion.

II. Basic Mechanics of the Variable Neutral-line Manipulator

A 1-D concept of a traditional snake-like manipulator is shown in Fig. 2. This structure is composed of a flexible backbone at the center with evenly placed disks [see the proximal part of Fig. 2(a)] [1], or multiple links with pivots at their centers, with springs fixed around them [see the distal part of Fig. 2(a)] [6]. They are actuated by a pair of wires placed at an equal distance from the center. Fig. 2(a) illustrates an example of the bent pose when the left-side wire is pulled and the other is loosened. If we assume that the compression of the backbone (or pivot mechanism) is negligible compared with bending, then the length of the centerline is invariant. The relationship between amount of the movement of the right and left wires Δl_r and Δl_l and the bending angle of the manipulator θ can be easily obtained as follows:

$$\Delta l_r = -\Delta l_l = \frac{w}{2}\theta \tag{1}$$

where w denotes the width between the left and right wires. This equation shows that the left and right wires have the same magnitude and opposite direction. This symmetric movement of wires provides an underactuated mode that introduces passive compliance, as mentioned in the previous section. When we consider a situation where the wires are fixed at a straight

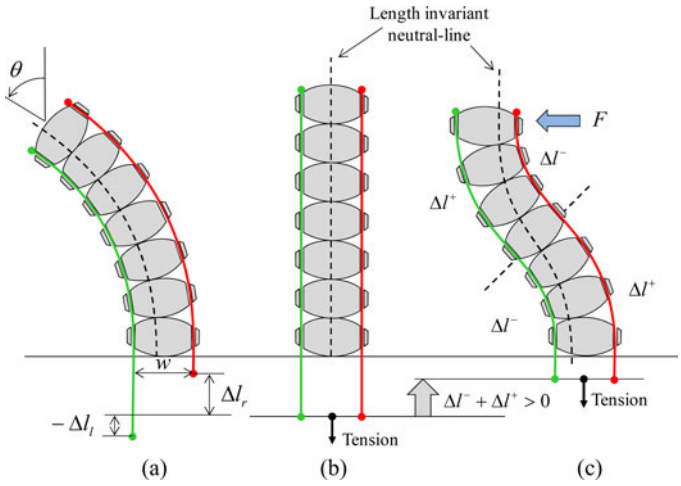

Fig. 3. One-dimensional concept of the variable neutral-line manipulator.

pose, as in Fig. 2(b), and an external force is applied to the lateral direction at the end of the manipulator, it tends to bend easily into to an s-shape regardless of wire tension, as shown in Fig. 2(c). This is because the manipulator can be moved to various configurations without changing the wire length. Therefore, the manipulator stiffness to resist bending comes solely from the fixed stiffness of the flexible backbone, or the springs, and not from wire tension.

Moreover, in order to obtain higher stiffness, stiffer materials must be used and, accordingly, a higher wire tension is needed to overcome the stiffness of the backbone or springs, which can lead to a reduction of available drive actuator force and a larger required wire diameter.

On the other hand, if asymmetric movement of the wire pair can be achieved, then the stiffness of the manipulator can be a function of the wire tension. Fig. 3 shows an example of an asymmetric mechanism. This mechanism employs self-similar links with rolling joints, instead of pivots or a backbone, where the joint has arc-shape contact surfaces. When it bends similar to as shown in Fig. 3(a), movement of the loosened wire Δl_r is longer than that of pulled wire Δl_l, which leads to asymmetric behavior. When a lateral force is applied, as shown in Fig. 3(c), the total movement of the wires $\Delta l^- + \Delta l^+$ has a positive value. This is important, since it implies that the proper tension of the wires dictates the force maintaining the shape of the manipulator. (A detailed analysis of the relationship between wire tension and stiffness of the manipulator will be investigated in Sections III and IV.) In contrast with traditional snake-like manipulators, the location of the length invariant neutral-line shown in Fig. 3 is not fixed at the center. In mechanics, neutral-line (or neutral surface) denotes a conceptual line within a beam or cantilever, where there is no compression or tension and thus the length does not change. As the position of the neutral-line varies according to the pose of the proposed mechanism, this device is termed a variable neutral-line manipulator.

The contact surface of the joint does not need to have a circular shape. Many other asymmetric joints can produce the variable stiffness property, but here, we will focus on the cylindrical

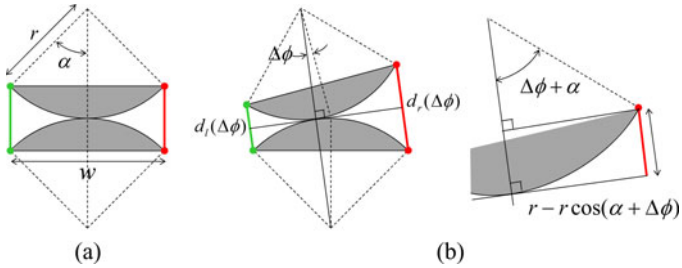

Fig. 4. Close-up view of the 1-D rolling joint.

rolling joint for simplicity and discuss other possibilities briefly in Section VII. In the remaining part of this section, the basic mechanics and the asymmetric property in the situation in which no external forces are described.

A. *One-Degree-of-FreedomVariable Neutral-Line Manipulator*

From the geometry of each joint, the relationship between the bending angle of the manipulator and the movement of the wires can be derived. If we assume that there is no external force, then the bending shape will be arc shapes, as in Fig. 3(a). Let us define n and $\Delta\phi$ as the number of joints (not links), and the bending angle of one joint with respect to the proximal link. As already defined, θ is the bending angle of the manipulator tip, and as the manipulator has an arc shape, we know that $\theta = n\Delta\phi$. Fig. 4 illustrates a close-up view of the rolling joint, where r, w, α, d_l, and d_r represent the radius of contact surface, the width between the left and right wires, half of the contact angle, and local length of the left and right wires, respectively. From Fig. 4(b), d_l and d_r can be calculated as follows:

$$d_l(\Delta\phi) = 2r\left(1 - \cos\left(\alpha - \frac{\Delta\phi}{2}\right)\right)$$
$$d_r(\Delta\phi) = 2r\left(1 - \cos\left(\alpha + \frac{\Delta\phi}{2}\right)\right). \quad (2)$$

Therefore, the movements of the left and right wires Δd_l and Δd_r are

$$\Delta d_l(\Delta\phi) \equiv d_l(\Delta\phi) - d_l(0) = 2r\left(\cos\alpha - \cos\left(\alpha - \frac{\Delta\phi}{2}\right)\right)$$
$$\Delta d_r(\Delta\phi) \equiv d_r(\Delta\phi) - d_r(0) = 2r\left(\cos\alpha - \cos\left(\alpha + \frac{\Delta\phi}{2}\right)\right). \quad (3)$$

Consequently, the relationship between θ and the overall length change of the left and right wires Δl_l and Δl_r, with no external force, can be obtained as (4). Here, we can notice that the sum of the length change is nonzero.

$$\Delta l_l(\theta) = n\Delta d_l = 2nr\left(\cos\alpha - \cos\left(\alpha - \frac{\theta}{2n}\right)\right)$$
$$\Delta l_r(\theta) = n\Delta d_r = 2nr\left(\cos\alpha - \cos\left(\alpha + \frac{\theta}{2n}\right)\right). \quad (4)$$

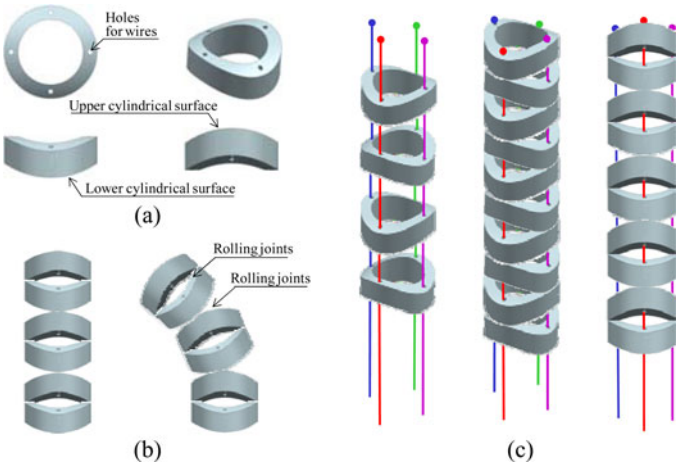

Fig. 5. Two-dimensional concept of the variable neutral-line manipulator. (a) Link shape. (b) Link connections. (c) 2-DOF manipulator.

B. Two-Degree-of-Freedom Variable Neutral-Line Manipulator

Fig. 5 illustrates a diagram of a 2-DOF manipulator. Each link shown in Fig. 5(a) has two cylindrical contact surfaces, oriented orthogonally to each other. At the center of the link there is a large hole, which distinguishes the device structurally from many other snake-like manipulators. The contact surfaces between adjacent links form rolling joints, and they are alternately placed at orthogonal directions to each other as shown in Fig. 5(b) and (c). In order to prevent slip between the rolling surfaces, flexures can be used which will be described in Section V and Fig. 14(b).

In the case of the 2-DOF manipulator, as shown in Fig. 6(b), there are two wire pairs, and the motion of the two pairs affects each other. In other words, when the manipulator is deflected by one wire pair's motion, the other wires placed at the center of links [the red line in Fig. 6(b)] are also pulled. Let us call the horizontal motion and vertical motion in Fig. 6(a) pan motion and tilt motion, respectively, and let the corresponding wire pairs be called the pan wire pair and tilt wire pair. The manipulator has the same number of links n for each pan motion and tilt motion. In addition, $\Delta\phi_p$ and $\Delta\phi_t$ denote bending angles for pan motion and tilt motion of a joint, and $\Delta d_{pl}, \Delta d_{pr}, \Delta d_{tl}$, and Δd_{tr} denote the displacements of the lengths of the pan wire pair and tilt wire pair of a joint, respectively. In a similar way as (3), the displacement of the pan wires can be calculated as follows:

$$\begin{aligned}&\Delta d_{pl}(\Delta\phi_p, \Delta\phi_t)\\&= 2r\left(\cos\alpha - \cos\left(\alpha - \frac{\Delta\phi_p}{2}\right) + 1 - \cos\frac{\Delta\phi_t}{2}\right)\\&\Delta d_{pr}(\Delta\phi_p, \Delta\phi_t)\\&= 2r\left(\cos\alpha - \cos\left(\alpha + \frac{\Delta\phi_p}{2}\right) + 1 - \cos\frac{\Delta\phi_t}{2}\right).\end{aligned} \quad (5)$$

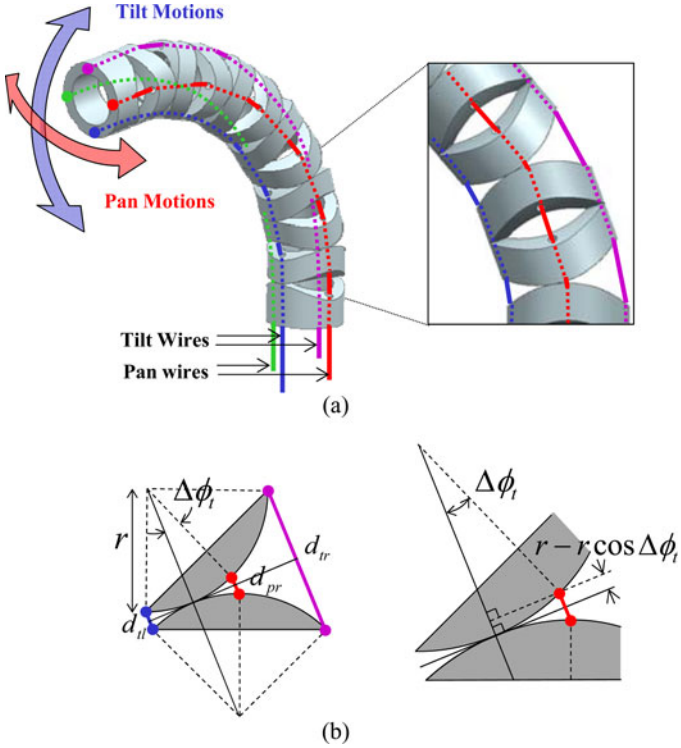

Fig. 6. (a) Pan motion and Tilt motion (b) Close-up view of tilting surface of 2-D variable neutral-line manipulator.

The term $1 - \cos(\Delta\phi_t/2)$ in (5) implies that the tilt motion contributes to the movement of the pan wires. It can be derived from the diagram of the rolling joint in Fig. 6(b). In a similar way as (4), the relationship between the angle of the end effector and the length change of the pan wires can be obtained as

$$\begin{aligned}\Delta l_{pl}(\theta_p, \theta_t) &= 2nr\left(\cos\alpha - \cos(\alpha - \frac{\theta_p}{2n}) + 1 - \cos\frac{\theta_t}{2n}\right)\\\Delta l_{pr}(\theta_p, \theta_t) &= 2nr\left(\cos\alpha - \cos(\alpha + \frac{\theta_p}{2n}) + 1 - \cos\frac{\theta_t}{2n}\right)\end{aligned} \quad (6)$$

where $\Delta l_{pl}, \Delta l_{pr}, \theta_p$, and θ_t denote the overall displacement of the left pan wire and right pan wire and the components of the end-effector tip angle in the directions of pan motion and tilt motion, respectively. These equations are valid when an external force does not exist, and the bending angle of each joint has the same angle. The relationship between the angle of the end effector and the length change of the tilt wires also can be calculated in the same way.

III. Deflection Characteristics Under External Force

In order to show that the stiffness of the manipulator is controllable by changing the wire tension, the bending shape of the manipulator under an external force will be calculated. In this paper, small deflections about the straight pose will be considered. The deflection diagrams [such as Figs. 3(c) and 7(a)] show an exaggerated shape for ease in explanation. Since we assume

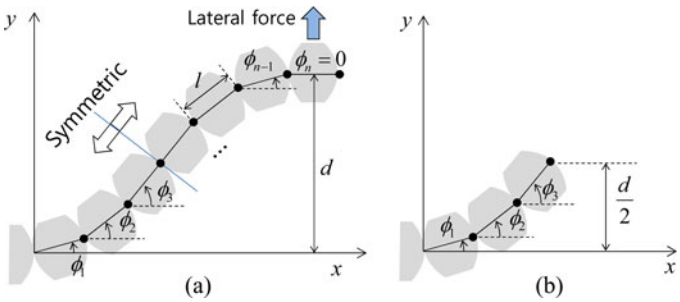

Fig. 7. Deflection model of the straight pose 1-DOF manipulator under a lateral force.

that the manipulator links are rigid, an axial force applied to the tip while at a straight pose causes no effect, and thus only lateral forces cause deflection. An analysis of the manipulator stiffness under an arbitrary bending angle and the effect of moment loading at the end effector are both beyond the scope of this paper. Therefore, we will focus on the analysis of manipulator deflection when subject to a lateral force.

Let us start with analysis of a 1-DOF manipulator. As shown in Fig. 7(a), the amount of lateral motion d generated by a lateral force in the y direction is

$$d = \sum_{i=1}^{n} l \sin \phi_i \tag{7}$$

where l, n, and ϕ_i denote the length of the links, number of joints, and the bending angle of the ith joint with respect to the x-axis. Note that ϕ_n is always zero. In the case of large deflections, the joints move differently from ordinary revolute joints, however since we only consider small motion, we approximate them as revolute joints. As the two wires are pulled to maintain a straight pose[see Fig. 3(c)], the movements of the left and right wires are the same, i.e.,

$$\Delta l_l = \Delta l_r. \tag{8}$$

The objective is to find the pose of the manipulator under lateral motion that minimizes the change of length of the wires. Therefore, the problem is to find the set of ϕ_i as follows:

$$\arg\min_{\phi} \left(\Delta l_l + \Delta l_r\right) \tag{9}$$

where ϕ denotes the set of ϕ_i, and thus it represents the deflected pose of the manipulator. Δl_l and Δl_r in (8) and (9) have different values than in (4) because the manipulator is subject to an external force, and thus angle ϕ_i in each link is different from each other. Thus, Δl_l and Δl_r should be calculated by summing the displacement of the wires of each link using (3).

$$\begin{aligned}\Delta l_l &= \sum_{i=1}^{n} \Delta d_l(\Delta\phi_i) = \sum_{i=1}^{n} 2r\left(\cos\alpha - \cos\left(\alpha - \frac{\Delta\phi_i}{2}\right)\right)\\ \Delta l_r &= \sum_{i=1}^{n} \Delta d_r(\Delta\phi_i) = \sum_{i=1}^{n} 2r\left(\cos\alpha - \cos\left(\alpha + \frac{\Delta\phi_i}{2}\right)\right)\end{aligned} \tag{10}$$

where $\Delta\phi_i = \phi_i - \phi_{i-1}, \phi_0 = 0$, and $\phi_n = 0$.

If we substitute (10) into (8), we find

$$\begin{aligned}&\sum_{i=1}^{n} 2r\left(\cos\alpha - \cos\left(\alpha - \frac{\Delta\phi_i}{2}\right)\right)\\ &= \sum_{i=1}^{n} 2r\left(\cos\alpha - \cos\left(\alpha + \frac{\Delta\phi_i}{2}\right)\right)\\ &\sum_{i=1}^{n}\left(\cos\left(\alpha + \frac{\Delta\phi_i}{2}\right) - \cos\left(\alpha - \frac{\Delta\phi_i}{2}\right)\right)\\ &= \sum_{i=1}^{n}\left(-2\sin(\alpha)\sin\left(\frac{\Delta\phi_i}{2}\right)\right) = 0.\end{aligned}$$

Because $\sin\alpha$ is nonzero, (8) is reduced to

$$\sum_{i=1}^{n} \sin\left(\frac{\Delta\phi_i}{2}\right) = 0. \tag{11}$$

In addition, the cost function $\Delta l_l + \Delta l_r$ in (9) can be simplified [using (10)] as

$$\begin{aligned}\Delta l_l + \Delta l_r &= 4nr\cos\alpha\\ &\quad - \sum_{i=1}^{n} 2r\left(\cos\left(\alpha + \frac{\Delta\phi_i}{2}\right) + \cos\left(\alpha - \frac{\Delta\phi_i}{2}\right)\right)\\ &= 4nr\cos\alpha - 4r\cos\alpha\sum_{i=1}^{n}\cos\left(\frac{\Delta\phi_i}{2}\right).\end{aligned} \tag{12}$$

Thus, the minimization problem (9) can be rewritten by a maximization problem. Consequently, we can obtain the optimization problem of (13) with the two constraints (7) and (11) as follows:

$$\arg\max_{\phi}\left(\sum_{i=1}^{n}\cos\left(\frac{\Delta\phi_i}{2}\right)\right) \tag{13}$$

such that

$$\sum_{i=1}^{n}\sin\phi_i = \frac{d}{l} \text{ and } \sum_{i=1}^{n}\sin\left(\frac{\Delta\phi_i}{2}\right) = 0.$$

For a more simplified formulation, it is worthwhile to consider the geometric property of a tendon-supported structure under lateral forces. The lateral force as shown in Fig. 7(a) generates a torque, or moment, at the proximal end of the manipulator, and the wire pair delivers the same amount of torque to the distal end [2]. As a result, the manipulator deflects into a symmetric s-shape, because the same amount of torque is applied at each end. Exploiting this property, the problem can be represented by half of the joint configuration of the manipulator, as shown in Fig. 7(b). This symmetric property can eliminate the constraint of (11), because the equality of the displacement of both wires (8) is automatically satisfied. $\Delta\phi_i$ is the change of ϕ_i, as shown in (10), and its sign could be either positive or negative depending on its location. For example, in Fig. 7(a), the lower half of the manipulator will always have positive $\Delta\phi_i$, while the upper half will have negative $\Delta\phi_i$.

A. Analysis of Manipulators With Odd Number of Joints

Therefore, in the case of an odd number of joints, the optimization function (13) and constraint (7) are rewritten as

$$\arg\max_{\phi}\left(\frac{1}{2}\cos\left(\frac{\Delta\phi_m}{2}\right)+\sum_{i=1}^{m-1}\cos\left(\frac{\Delta\phi_i}{2}\right)\right) \tag{14}$$

such that

$$\sum_{i=1}^{m-1}\sin\phi_i=\frac{d}{2l} \tag{15}$$

where $\Delta\phi_i=\phi_i-\phi_{i-1}, \phi_0=0$, and $m=(n+1)/2$.

Due to the assumption of small deflections, the trigonometric function in (14) and (15) can be approximated using a Taylor series expansion as

$$\begin{aligned}&\frac{1}{2}\cos\left(\frac{\Delta\phi_m}{2}\right)+\sum_{i=1}^{m-1}\cos\left(\frac{\Delta\phi_i}{2}\right)\\&=\frac{1}{2}\left(1-\frac{1}{8}\Delta\phi_m^2\right)+\sum_{i=1}^{m-1}\left(1-\frac{1}{8}\Delta\phi_i^2\right)\\&=\left(m-\frac{1}{2}\right)-\frac{1}{8}\left(\frac{1}{2}\Delta\phi_m^2+\sum_{i=1}^{m-1}\Delta\phi_i^2\right)\end{aligned}$$

and

$$\sum_{i=1}^{m}\sin\phi_i=\sum_{i=1}^{m}\phi_i.$$

In order to solve this approximate optimization problem, the method of Lagrange multipliers is applied. The Lagrange function is defined as

$$\Lambda(\phi)=f(\phi)+\lambda g(\phi) \tag{16}$$

where

$$f(\phi)=\frac{1}{2}\Delta\phi_m^2+\sum_{i=1}^{m-1}\Delta\phi_i^2,\quad g(\phi)=\left(\sum_{i=1}^{m}\phi_i\right)-\frac{d}{2l}$$

and λ is a Lagrange multiplier. $f(\phi)$ again represents the minimization function, because the sign is changed during approximation. Differentiating (16), the following necessary conditions for the solution are obtained:

$$\frac{\partial\Lambda(\phi)}{\partial\phi_i}=\begin{cases}4\phi_i-2\phi_{i+1}+\lambda=0, & i=1\\-2\phi_{i-1}+4\phi_i-2\phi_{i+1}+\lambda=0, & 1<i<m-1\\-2\phi_{i-1}+3\phi_i-\phi_{i+1}+\lambda=0, & i=m-1\\-\phi_{i-1}+\phi_i=0, & i=m\end{cases} \tag{17}$$

$$\frac{\partial\Lambda(\phi)}{\partial\lambda}=\sum_{i=1}^{m-1}\phi_i-\frac{d}{2l}=0. \tag{18}$$

These can be expressed in a matrix form as

$$\underbrace{\begin{bmatrix}4&-2&&&&&1\\-2&4&-2&&&&1\\&-2&4&-2&&&1\\&&\ddots&\ddots&\ddots&&\vdots\\&&&-2&3&-1&1\\&&&&-1&1&0\\1&1&1&\dots&1&0&0\end{bmatrix}}_{\equiv A}\begin{bmatrix}\phi_{m\times1}\\\lambda\end{bmatrix}=\underbrace{\begin{bmatrix}0_{m\times1}\\d/2l\end{bmatrix}}_{\equiv c} \tag{19}$$

where we call the $m+1$ by $m+1$ matrix on the left side A, and the $m+1$ vector on the right side c. In the case of 3-joint manipulators (i.e. $n=3$), A and c are

$$A|_{n=3}=\begin{bmatrix}3&-1&1\\-1&1&0\\1&0&0\end{bmatrix}\text{ and }c=\begin{bmatrix}0\\0\\d/2l\end{bmatrix}. \tag{20}$$

As a result, the deflected pose (i.e., the set of ϕ_i) can be obtained from the following equation:

$$\begin{bmatrix}\phi\\\lambda\end{bmatrix}=A^{-1}c. \tag{21}$$

B. Analysis of Manipulators With Even Number of Joints

Until now, we have considered the case of manipulators with an odd number of joints. In the case of an even number of joints, the symmetric property can be used similarly, if we take into account that the distal link of the simplified model has half the size of the other links.

In a similar derivation as (14) and (15), the optimization problem for a manipulator with an even number of joints is

$$\arg\max_{\phi}\left(\sum_{i=1}^{m}\cos\left(\frac{\Delta\phi_i}{2}\right)\right) \tag{22}$$

such that

$$\frac{1}{2}\sin\phi_m+\sum_{i=1}^{m-1}\sin\phi_i=\frac{d}{2l} \tag{23}$$

where $\Delta\phi_i=\phi_i-\phi_{i-1}, \phi_0=0$, and $m=n/2$.

The equation (21) can be used to find a solution for an even number of joints, where the matrix A takes on unique values, as

$$A|_{\text{even links}}=\begin{bmatrix}4&-2&&&&1\\-2&4&-2&&&1\\&\ddots&\ddots&\ddots&&\vdots\\&&-2&4&-2&1\\&&&-2&-2&1/2\\1&1&\cdots&1&1/2&0\end{bmatrix}. \tag{24}$$

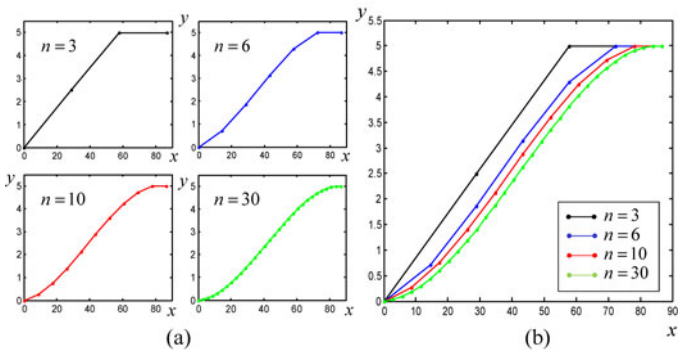

Fig. 8. Deflected shapes of simulated manipulators.

In the case of 4-joint manipulators (i.e. $n = 4$), A is

$$A|_{n=4} = \begin{bmatrix} 4 & -2 & 1 \\ -2 & -2 & 1/2 \\ 1 & 1/2 & 0 \end{bmatrix}.$$

In the case of two-joint manipulators (i.e., $n = 2$), the set of ϕ_i can be directly calculated from (7) as $\phi_1 \cong d/l$ and $\phi_2 = 0$.

Fig. 8 shows the deflected shapes of various simulated manipulators according to their number of links. The length of the manipulator nl, radius of contact surface r, half of the contact surface angle α, and amount of the lateral displacement d are 87 mm, 14.8 mm, 33.18°, and 5 mm, respectively.

C. Two-Degrees-of-Freedom Analysis

In order to extend these analyses to a 2-DOF manipulator, the coupling term $1 - \cos(\Delta\phi_t/2)$ in (5) should be considered. Let us consider a situation of a 2-DOF manipulator where the external force in the pan direction results in a deflecting motion in the same direction. Then, the displacements of pan wires are the same as (10) because the tilt angle of each joint is zero. However, the displacements of the tilt wires are nonzero due to the coupling term, as follows:

$$\begin{aligned} \Delta l_{tl} &= \sum_{i=1}^{n} 2r\left(\cos\alpha - \cos\left(\alpha - \frac{\Delta\phi_{ti}}{2}\right) + 1 - \cos\frac{\Delta\phi_{pi}}{2}\right) \\ &= \sum_{i=1}^{n} 2r\left(1 - \cos\frac{\Delta\phi_{pi}}{2}\right) \\ \Delta l_{tr} &= \sum_{i=1}^{n} 2r\left(\cos\alpha - \cos\left(\alpha + \frac{\Delta\phi_{ti}}{2}\right) + 1 - \cos\frac{\Delta\phi_{pi}}{2}\right) \\ &= \sum_{i=1}^{n} 2r\left(1 - \cos\frac{\Delta\phi_{pi}}{2}\right) \end{aligned} \tag{25}$$

where $\Delta l_{tl}, \Delta l_{tr}, \Delta\phi_{pi}$ and $\Delta\phi_{ti}$ denote displacements of the left and right tilt wires and the pan and tilt angle of i th link, respectively, and $\Delta\phi_{ti}$ is zero because there is no tilt motion.

Here, the objective is to find the pose of the manipulator (i.e., the set of ϕ_{pi}) when subjected to lateral loading that minimizes the change of lengths of the tilt wires, as well as that of the pan wires. If we consider the minimization problem for only the tilt wires:

$$\arg\min_{\phi_p} \left(\Delta l_{tl} + \Delta l_{tr}\right). \tag{26}$$

From (25) and (26), the optimization problem is rewritten as

$$\arg\max_{\phi_p} \left(\sum_{i=1}^{n} \cos\left(\frac{\Delta\phi_{pi}}{2}\right)\right). \tag{27}$$

Note that (27) for the tilt wires has exactly the same cost function as that of the pan wires (13). This is important because it implies that displacing the tilt wires under lateral loading produces the same deflected pose as displacing the pan wires. It also means that (13) represents the optimization problem for the 2-DOF manipulator. Therefore, the deflected shape obtained from (21) can be applied directly to the 2-DOF manipulator.

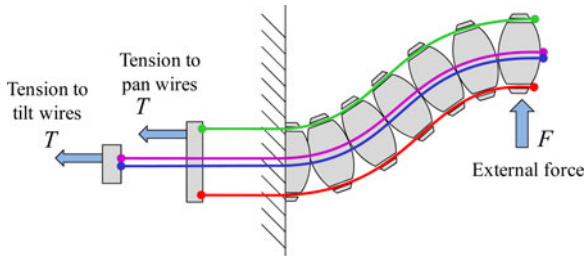

Fig. 9. Schematic of tensions and force exerted in a 2-DOF manipulator.

IV. Stiffness of the Variable Neutral-Line Manipulator

In this section, the relationship between the stiffness of the manipulator and the wire tension is calculated by using the deflected shape obtained in the previous section. Fig. 9 shows a schematic of the wire tensions and force exerted on the manipulator, where the same tension T is applied to the pan wires and tilt wires individually, and F is the external lateral force applied to the end effector. The tensioning mechanism is highly simplified here, and the detailed structure will be described in Section V.

For clarity of the stiffness calculations, let us first define several terms. In (21), only c contains design parameters l and d. Thus, we can cancel out these design parameters by defining the following variable:

$$s_i = \frac{nl}{d}\phi_i = \frac{h}{d}\phi_i \tag{28}$$

where $h{=}nl$ and can be considered as the total length of the manipulator. The set of s_i can be calculated by substituting ϕ_i in (21) with (28), i.e.,

$$\begin{bmatrix} s_i|_{m\times 1} \\ \lambda \end{bmatrix} = A^{-1}\begin{bmatrix} 0_{m\times 1} \\ n/2 \end{bmatrix} \tag{29}$$

which shows that s_i is a design-independent constant related only to the number of the joints n. Using this relationship, we can define another constant

$$S_n \equiv n\sum_{i=1}^{n} \Delta s_i^2 \tag{30}$$

TABLE I
DESIGN-INDEPENDENT STIFFNESS COEFFICIENT

n	2	3	4	5	6	10	30	∞
S_n	16.00	13.50	12.80	12.50	12.34	12.12	12.01	12.00

where $\Delta s_i = s_i - s_{i-1}, s_0 = 0$. The values of S_n shown in Table I were calculated by using (29) and (30) for each case of n. They are also design-independent parameters only related to n, regardless of the link length l, radius of contact surface r, or half of the contact surface angle α.

Now, it is possible to derive the stiffness of the variable neutral-line manipulator. From (12), the displacement of the pan wires Δl_p can be expressed as follows:

$$\begin{aligned}\Delta l_p &\equiv \Delta l_{pl} = \Delta l_{pr} = (\Delta l_{pl} + \Delta l_{pr})/2 \\ &= 2nr\cos\alpha - 2r\cos\alpha \sum_{i=1}^{n} \cos\left(\frac{\Delta\phi_i}{2}\right) \\ &\cong 2nr\cos\alpha - 2r\cos\alpha \sum_{i=1}^{n} \left(1 - \frac{1}{8}\Delta\phi_i^2\right) \\ &= \frac{r\cos\alpha}{4} \sum_{i=1}^{n} \Delta\phi_i^2. \end{aligned} \tag{31}$$

By substituting (28)–(30) into (31), the relationship between d and Δl_p can be calculated as

$$\Delta l_p = \frac{r\cos\alpha}{4} \sum_{i=1}^{n} \left(\left(\frac{d}{h}\right)^2 \Delta s_i^2\right) = S_n \frac{r\cos\alpha}{4nh^2} d^2. \tag{32}$$

From (25), the displacement of the tilt wires Δl_t can also be expressed as follows:

$$\begin{aligned}\Delta l_t &\equiv \Delta l_{tl} = \Delta l_{tr} = 2r \sum_{i=1}^{n} \left(1 - \cos\left(\frac{\Delta\phi_i}{2}\right)\right) \\ &\cong 2r \sum_{i=1}^{n} \left(\frac{1}{8}\Delta\phi_i^2\right) = \frac{r}{4} \sum_{i=1}^{n} \left(\left(\frac{d}{h}\right)^2 \Delta s_i^2\right) = S_n \frac{r}{4nh^2} d^2. \end{aligned} \tag{33}$$

By using the virtual work concept, an energy conservation equation can be obtained as follows:

$$\int_0^d F dx = T\Delta l_p + T\Delta l_t. \tag{34}$$

By putting (32) and (33) into (34) and differentiating both sides of (33) by d

$$F = TS_n \frac{r\cos\alpha}{4nh^2} 2d + TS_n \frac{r}{4nh^2} 2d. \tag{35}$$

As a result, the stiffness K is obtained as

$$K = \frac{F}{d} = S_n \frac{r(1+\cos\alpha)}{2nh^2} T. \tag{36}$$

This verifies that the stiffness of the manipulator can be adjusted via the tension of the wires, and the relationship between the stiffness and the tension is approximately linear. This is an important advantage of the variable neutral-line design compared with other comparable manipulators. Note that increasing the number of joints reduces the manipulator stiffness because n is in the denominator of (36). However, if the maximum bending angle is considered, this leads to a different conclusion, which will be discussed in Section VII-B.

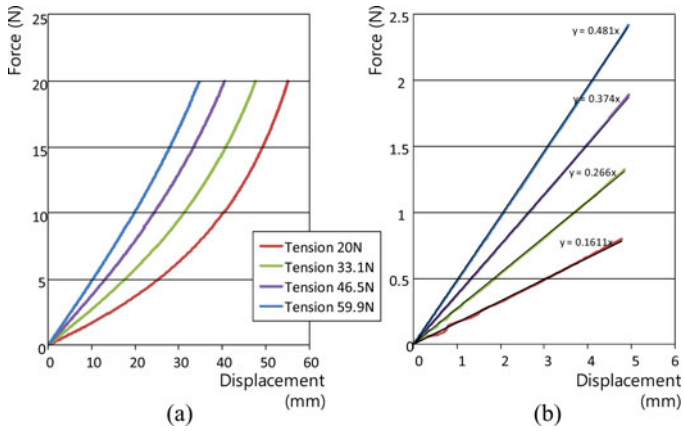

Fig. 10. Stress–strain graph as determined by simulation. (a) Overall shape of graph. (b) Close-up shape near zero.

TABLE II
SPECIFICATIONS OF THE 2-DOF MANIPULATOR

Specification	Value
Number of Joints n	3
Half of Contact angle α	0.579 rad
Radius of Contact surface r	14.8 mm
Link Length l	29 mm
Pretension (N)	20.0, 33.1, 46.5, 59.9 N

TABLE III
STIFFNESS COMPARISON

Tension (N)	20.0	33.1	46.5	59.9
Simulated Stiffness (N/mm)	0.161	0.266	0.374	0.481
Calculated Stiffness (N/mm)	0.162	0.268	0.376	0.484

Fig. 10 illustrates the simulation results of the manipulator with the specification of Table II, where frictional effects are ignored. For the simulation, the multibody dynamics simulation software MSC ADAMS 2012 was used. When the maximum lateral motion in Fig. 10(a) is extremely high (more than 60 mm in minimum tension), the overall graph does not follow a linear relationship because the manipulator behavior lies outside the valid range of the Taylor series approximations applied to (14), (15), (22), and (23). However, in a reasonably small region about zero displacement, it shows an approximately linear relationship. Table III shows the simulated stiffness and calculated stiffness using (36). The error between them is negligible, which means that the stiffness calculation and approximation is valid.

V. ACTUATION SYSTEM DESIGN

Most current tendon-driven mechanisms employ pulley mechanisms or linear actuators, due to the symmetric property of the wire pair. Fig. 11(a) shows a concept of an actuator design using a pulley mechanism. This simple approach cannot

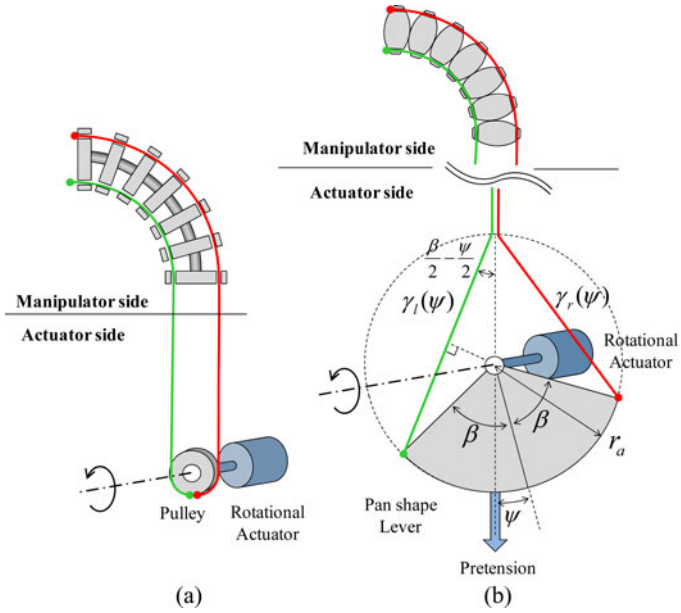

Fig. 11. Conceptual Design of Actuating Mechanisms. (a) Conventional concept (b) Proposed concept.

be easily applied to the variable neural-line manipulator because it has an asymmetric wire movement. If the pulley mechanism is used for the variable neutral-line manipulator, the pulley is pulled as it deflects, which means that the pivot of the pulley moves in a wide range, and the wire tension affects the torque of the actuator when it bends. Alternatively, two linear actuators can be used to actuate two wires individually, but these actuators must have a complex force control function for tension control.

Therefore we propose a new actuation mechanism that mechanically compensates for the asymmetric wire movement, and achieves a proportional relationship between actuator motion and manipulator motion. Fig. 11(b) shows the basic concept of the proposed actuation mechanism for a 1-DOF manipulator. It is composed of a fan-shaped lever and an actuator wire pair connected at both the ends of the lever.

The length of the actuator wire pair γ_l and γ_r is obtained from Fig. 11(b) as follows:

$$\gamma_l(\psi) = 2r_a \sin\left(\frac{\pi-\beta+\psi}{2}\right) = 2r_a \cos\left(\frac{\beta}{2}-\frac{\psi}{2}\right)$$
$$\gamma_r(\psi) = 2r_a \sin\left(\frac{\pi-\beta-\psi}{2}\right) = 2r_a \cos\left(\frac{\beta}{2}+\frac{\psi}{2}\right) \quad (37)$$

where r_a, β, and ψ denote the radius of the lever, half of the pan shape angle, and the amount of lever rotation, respectively. The displacements of the actuator wire pair $\Delta\gamma_l$ and $\Delta\gamma_r$ are

$$\Delta\gamma_l(\psi) = \gamma_l(\psi) - \gamma_l(0) = -2r_a\left(\cos\left(\frac{\beta}{2}\right) - \cos\left(\frac{\beta}{2}-\frac{\psi}{2}\right)\right)$$
$$\Delta\gamma_r(\psi) = \gamma_r(\psi) - \gamma_r(0) = -2r_a\left(\cos\left(\frac{\beta}{2}\right) - \cos\left(\frac{\beta}{2}+\frac{\psi}{2}\right)\right). \quad (38)$$

Similarity between (4) and (38) shows that the proposed actuation mechanism can compensate the asymmetric motion of the wire pair. If we set the length of lever r_a as nr and half of the pan shape angle β as 2α, then the rotation of the lever and the bending angle of the manipulator has a direct relation $\psi = \theta/n$. Thus, the rotational actuator can solely control the bending motion of the manipulator, and the pretension shown in Fig. 11(b) can adjust the stiffness independently.

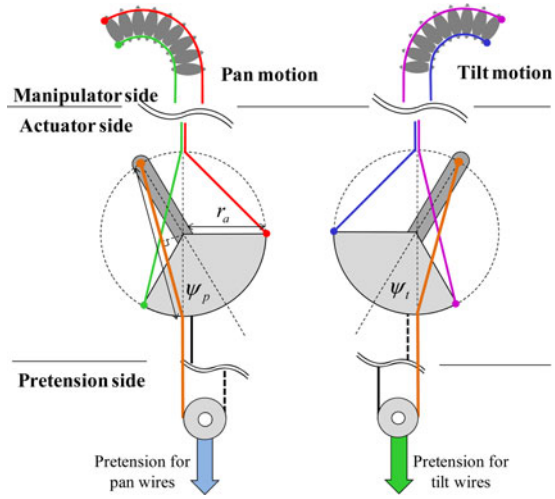

Fig. 12. Conceptual Design of 2-DOF Manipulator.

This actuation mechanism is for a 1-DOF manipulator. For complete compensation of 2-DOF motion as (6), another mechanism is required. Fig. 12 shows the actuation mechanism for a 2-DOF manipulator. The length of the brown colored wire changes as the lever rotates, as follows:

$$\Delta\nu(\psi_p) = 2r_a \cos\frac{\psi_p}{2}. \quad (39)$$

Similar to (38), it can compensate the last term of (6) if we set r_a and β as nr and 2α. Even though the proposed mechanism in Fig. 12 can compensate for the coupling of the 2-DOF manipulator, it can be somewhat complicated to implement. In Section VII-C, simplification of the actuator will be discussed.

A. *Implementation Details*

As illustrated in the conceptual designs in Figs. 11(b) and 12, the pivots of the actuation levers must be able to translate in order to deliver a pretension force to the wires through the lever mechanism. This moving pivot leads to a complicated implementation, because the gears and motors (with associated cabling) connected to the lever must all move along with the pivot motion. In order to simplify this, the wire path is redirected as shown in Fig. 13(a). Instead of moving the pivot of the lever, an additional pulley with a slider at the center moves according to the motion of the pretension wire (shown by the black solid line).

Fig. 13(b) and (c) shows a front and exploded views of the detailed actuator mechanical design. It is designed to satisfy the performance specifications in Table II. Two identical mechanisms are mounted in order to actuate one 2-DOF manipulator. For actuation of the levers, two 8-W BLDC motors with 53:1 gear heads were used. Between the levers and the gear heads,

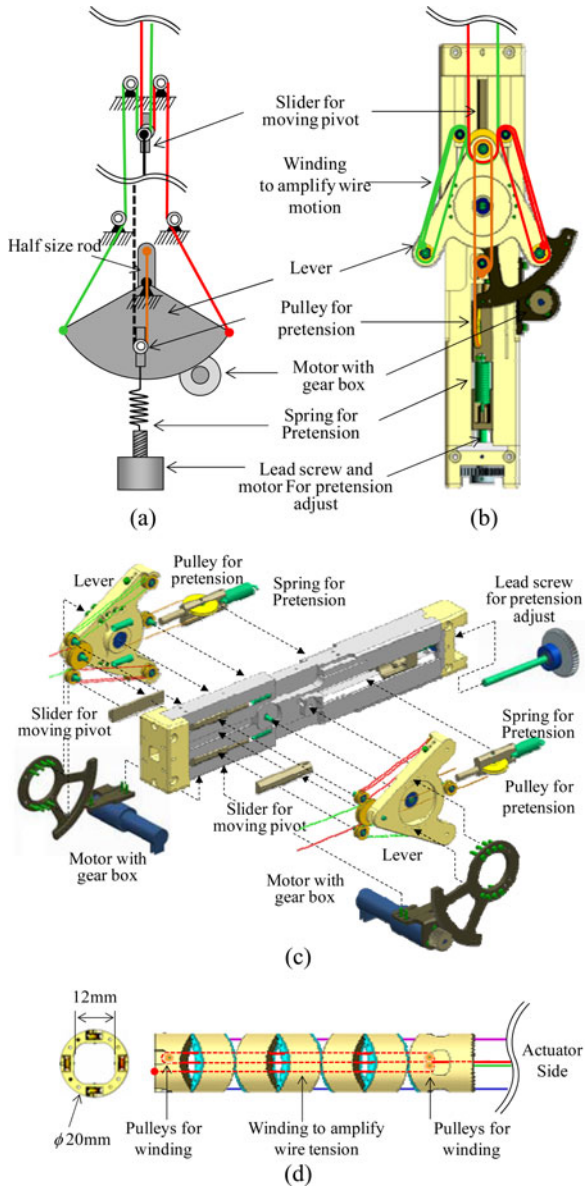

Fig. 13. Detailed Design of a 2-DOF Manipulator.

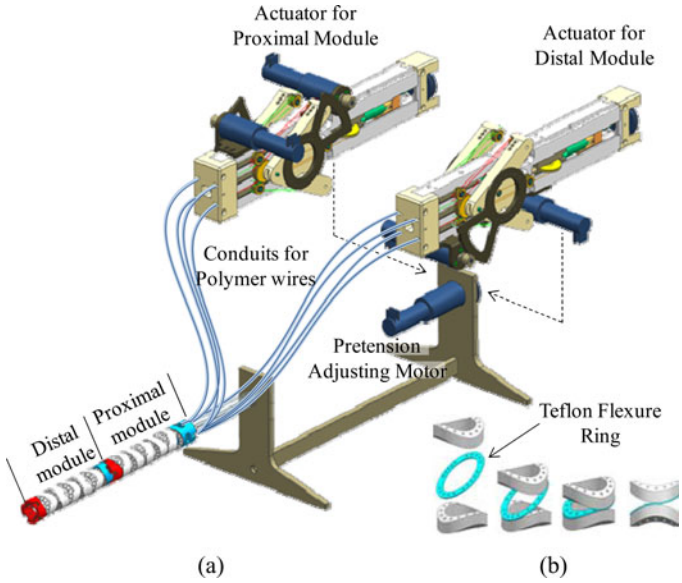

Fig. 14. Detailed design of 2-module 4-DOF manipulator.

8:1 gear pairs were placed. As the maximum continuous torque of the motor is 8 m·Nm and the efficiency of the gear head is 59%, the approximate continuous output torque of the lever is 2 Nm. In order to control the wire tensions, 1.22-mm pitch lead screws and springs were used. The tension can be changed from 8.8 to 40 N by rotating the lead screws using another geared motor having the same specification.

As can be seen in Fig. 13(b), the wires connected to the lever are wound three times around pulleys to amplify the wire motion. In order to minimize friction, miniaturized bearings were used for the pulleys. The wires connected to the manipulator shown in Fig. 13(d) are also wound three times to lessen the wire motion and amplify their tension. This amplification mechanism distributes the stress among multiple wires; hence, high tension for the manipulator can be achieved by using low-payload, small wires. For implementation, Polymer wires (Dyneema) of diameter 0.3 mm were used. However, amplifying the tension by using multiple windings also increases friction, and causes error between the modeling and implemented system due to hysteresis in repeated motion. This will be examined in Section VI.

Fig. 14(a) illustrates the assembled structure of a 4-DOF variable neutral-line manipulator system. Two identical 2-DOF manipulators were stacked, and two identical actuation mechanisms were connected to them. In order to transfer wire motion through a flexible path, teflon conduits were used. Fig. 14(b) shows the assembled structure of the joint. In order to make the joint exhibit pure rolling, teflon flexure rings of 0.5 mm thickness were attached between the links, as shown in Fig. 14(b). Most of large frames (made from ABS material) were fabricated mainly by using 3-D fused deposition manufacturing (FDM). Small parts like pulleys and sliders were made from aluminum alloy (AL 6061T6).

The diameter of the manipulator was chosen with a large inner channel to allow the passage of multiple dexterous surgical instruments and an endoscope. Theoretically, based on the design of the device, there are no strict size limitations. We expect that 5 and 3 mm diameters are also feasible, which are standard sizes of conventional laparoscopic surgical instruments. However, we note that as the device size shrinks, the payload and the stiffness will decrease accordingly.

Considering practical implementation issues, small-sized manipulators pose greater fabrication difficulties, such as fabricating miniaturized flexures and attaching them to rolling links. We can greatly simplify the mechanism by removing the flexure and allowing the actuation wires to replace the function of the flexure by guiding the rolling action between the link surfaces. However, the wires cannot completely prevent slip between the rolling surfaces, which could lead to inaccuracy in pose control.

The manipulator was designed for multiple uses. Sterilization is an important issue for such a complicated mechanism.

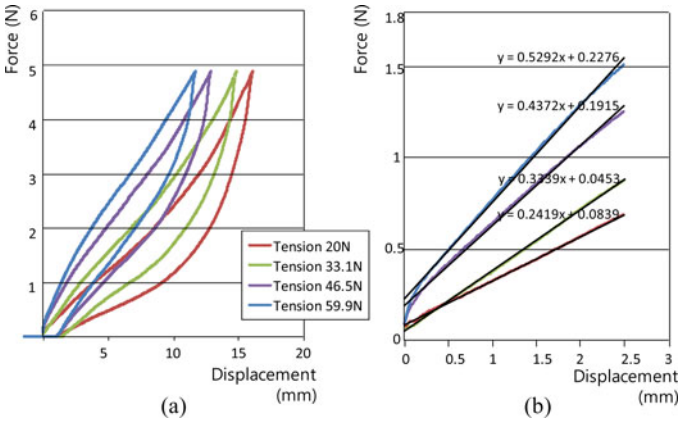

Fig. 15. Stress–strain graph by experiments. (a) Overall shape of graph. (b) Closed-up shape near zero.

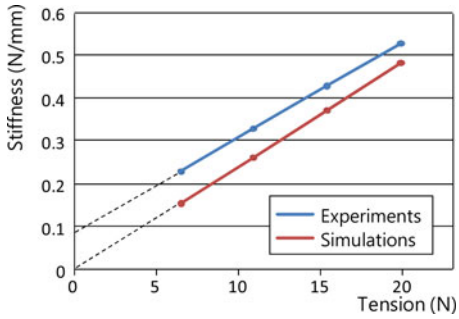

Fig. 16. Relationship between wire tension and manipulator stiffness.

TABLE IV
STIFFNESS BY EXPERIMENTS

Tension (N)	20.0	33.1	46.5	59.9
Stiffness (N/mm)	0.242	0.334	0.437	0.529

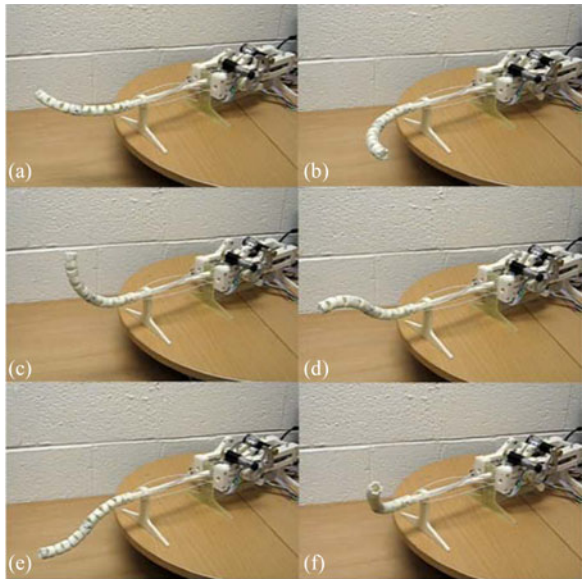

Fig. 17. Two-DOF manipulator prototype performing controlled motions.

We are considering low-temperature liquid sterilization methods because the mechanism has heat-sensitive components, and thus steam sterilization is not adequate. For the manipulator shown in Fig. 1(b), a cover sheath made from EPDM has been developed (not shown in the figure), which is a commonly used material for flexible endoscopes. In order to prevent the EPDM sheath being caught between the rolling surfaces and minimize friction between the sheath and manipulator, a mesh layer made by woven steel wires was placed between the sheath and the manipulator. However, the sheath acts to resistant bending motion and thus slightly increases hysteresis of the manipulator motion.

VI. Experimental Validation

This section presents experimental results to verify the proposed manipulator models. The experiments were conducted using the same specifications as those in Table II. The stiffness measurement was done on one module by using a texture analyzer which can measure up to a 49 N maximum force with 0.001 N sensitivity.

Fig. 15 illustrates the stress–strain curves measured for four different wire tensions levels. Although the lateral motion is relatively small compared with the simulation in Fig. 10, the curves are nonlinear and exhibit hysteresis behavior. The hysteresis is caused by changes in the wire tension according to the direction of frictional forces acting on the wires. When the manipulator is driven by an external force, friction aids the wire tension, and thus the manipulator exhibits higher stiffness. When the manipulator is driving itself, on the other hand, friction reduces the wire tension, and thus, the manipulator exhibits lower stiffness.

Sources of friction in the manipulator include a (relatively small) contribution from the bearings that accompany every pulley in the actuation mechanism. Moreover, the multiple windings of the wires in the manipulator not only amplify the wire tension, but also amplify the friction. Therefore, using a single wire for the manipulator, as shown in Fig. 6(a), instead of multiple windings, can reduce the hysteresis. However, in that scenario, thicker wires and conduits should be used to maintain a high payload. Applying teflon coating or inserting teflon tubes throughout the wire paths in the link holes of the manipulator could also reduce the friction and the resultant hysteresis.

The stiffness change according to the tension variation is approximately linear as shown in Fig. 16 and Table IV. The simulated stiffness–tension curve is linear, and crosses the zero point because it has no friction and follows (36). In contrast, the experimental curve has a nonzero y-intercept of 0.088 N/mm. It means that the additional force caused by friction aids the wire tension.

Fig. 17 shows several snapshots of motion of a 4-DOF variable neutral-line manipulator system prototype. As the maximum bending angle of one module is more than 45°, the manipulator can be bent 90° as shown in Fig. 17(a)–(c). Under no external force, the motion is not affected by the stiffness changes, and the motion with low stiffness is approximately the same as the motion with high stiffness.

VII. Discussion

So far, the mechanics of the variable neutral-line manipulator and the actuation mechanism have been investigated and verified. In this Section, the effect of joint number and design variations are discussed.

A. Maximum Bending Angle

As mentioned in Section VI, the maximum bending angle of one module is approximately 45°. This can be predicted by considering the tension balance. Let us consider the extreme bending pose of pan motion like shown in Fig. 6(b). In this extreme case, the left pan wire (shown by the blue line) has tension T, and the right pan wire (shown by the purple line) has zero tension, because the sum of the tilt wires have tension T, and this balances with the left pan wire. Therefore, the joint will be settled at the middle of the left pan wire and tilt wire at the center, which means that the maximum bending angle is half of α. Thus the maximum bending angle of the module is

$$\theta_{\max} = \frac{n\alpha}{2}. \tag{40}$$

The theoretical maximum bending angle of the implemented manipulator is 49.8°, which agrees reasonably with the measured value.

B. Stiffness Change With Joint Number Under Fixed Maximum Bending Angle and Link Width

Assuming that the maximum bending angle $\theta_{\max}$ and the width of the link w in Fig. 4(a) are fixed, we can see that the stiffness changes as the number of links increases using (36) and (40). These assumptions can be represented as

$$\theta_{\max} = \frac{n\alpha}{2} = \frac{n_i\alpha_i}{2} \tag{41}$$

$$\frac{w}{2} = r\sin\alpha = r_i\sin\alpha_i \tag{42}$$

where r_i and α_i are design parameters of an n_i-joint manipulator having the same maximum bending angle and link width. The stiffness of the n_i-joint manipulator is represented using (41) and (42) as

$$K_{n_i} = S_i\frac{r_i(1+\cos\alpha_i)}{2n_ih^2}T = S_i\frac{r\sin\alpha(1+\cos(n\alpha/n_i))}{2h^2n_i\sin(n\alpha/n_i)}T. \tag{43}$$

If we consider a manipulator with a large number of joints

$$K_\infty = \lim_{n_i\to\infty} K_{n_i} = S_\infty\frac{r\sin\alpha}{nh^2\alpha}T. \tag{44}$$

For example, the stiffness of the manipulator with an infinite number of joints is 0.445 N/mm when the tension is 59.9 N. This value is not severely small compared with the stiffness of the manipulator with three joints, which is 0.484 N/mm. It means that increasing joint number does not significantly affect the stiffness performance, and we can select the proper number of joints, depending on specific task requirements.

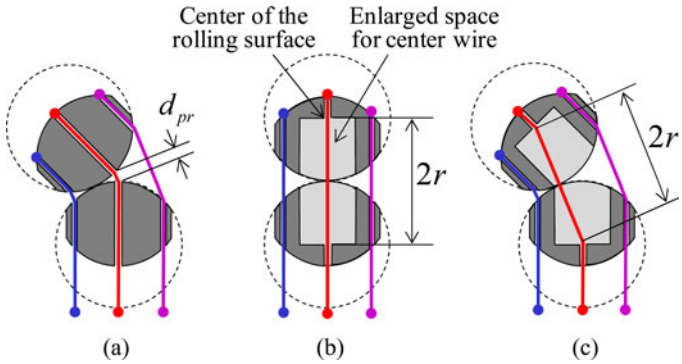

Fig. 18. (a) Original Link design and (b) and (c) modified link design to diminish the coupling between pan and tilt motion.

C. Simplification of Actuation Mechanism

In Section V, an actuation mechanism that completely compensates for the coupling of the 2-DOF manipulator was proposed. In order to simplify the actuation mechanism, two 1-DOF actuation mechanisms shown in Fig. 11(b) can be used for a 2-DOF manipulator if we can eliminate the coupling mechanically. Fig. 18 introduces a linkage design to diminish or eliminate the coupling effect. If we enlarge the space for passage of the center wire, then elongation of the center wire path is diminished or completely eliminated. Fig. 18(b) and (c) shows the linkage with space to the center of the rolling space, where the length of the wire path in the space is maintained, while the original link has additional length, as shown in Fig. 18(a). However, due to the removal of Δl_t shown in (33), the stiffness decreases as follows:

$$K = \frac{F}{d} = S_n\frac{r\cos\alpha}{2nh^2}T. \tag{45}$$

For practical use, this modification will be an efficient tradeoff between simplicity and performance.

D. Design Variation

As mentioned in Section II, the joint shape does not need to be a cylindrical-shape rolling mechanism. For instance, if the sum of wire movement has a negative value, then we can also control the stiffness by using pushing shafts instead of using pulling wire tension. However, in this case the actuation mechanism should be redesigned to compensate for asymmetric wire motion.

Fig. 19 presents two design variations of the proposed manipulator. In most cases of snake-like manipulators, the initial pose is straight shape, which represents a singular point. As shown in Fig. 17(a), the initial pose can be changed to a C-shape or S-shape by simply changing the individual link shape. In addition, by using different surface angles as Fig. 17(b), a near-rigid joint design is feasible. This manipulator can be inserted through a curved path by loosening the wire tension and can be used like a rigid joint by applying wire tension.

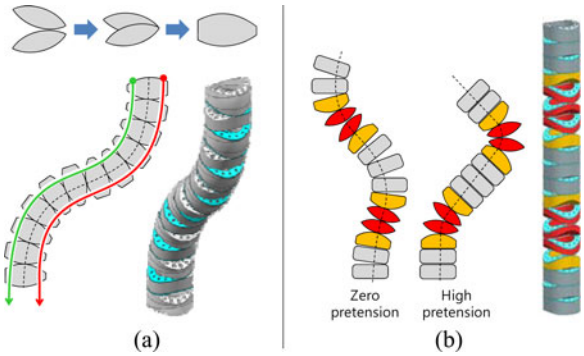

Fig. 19. (a) Precurved design. (b) Rigid-joint like design.

VIII. Conclusion

This paper introduced a unique variable neutral-line manipulator and actuation mechanism to achieve a controllable stiffness capability. Design, modeling, analysis, and experimental results of the variable neutral-line manipulator were presented. Detailed analysis of its stiffness properties and verification of its performance based on simulations and experiments proved the direct relationship between the wire tension and the stiffness of the manipulator, as well as its demonstrated stiffness controlling capability without losing motion control performance. The thin tubular structure of the manipulator and the ability to control the stiffness by only using position-controlled actuators could make the manipulator well suited for MIS applications. For instance, the manipulator can be used as a flexible guide tube of a single-port surgical device. In this application, the stiffness changing capability can be a great advantage, because compliance is important for safely moving the guide tube in the abdominal cavity. On the other hand, high stiffness is crucial for payload motion or precise operation.

Current study has been focussed on integrating all of these efforts to develop an innovative surgical robotic system and evaluating its performance and effectiveness. For future research, stiffness analysis under arbitrary bending angles will be investigated. For more precise position control, friction modeling and analysis deserve to be studied.

References

[1] J. Ding, K. Xu, R. Goldman, P. Allen, D. Fowler, and N. Simaan, "Design, simulation and evaluation of kinematic alternatives for insertable robotic effectors platforms in single port access surgery," in *Proc. IEEE Int. Conf. Robot. Autom.*, 2010, pp. 1053–1058.

[2] I. Gravagne and I. Walker, "Manipulability, force, and compliance analysis for planar continuum manipulators," *IEEE Trans. Robot. Autom.*, vol. 18, no. 3, pp. 263–273, Jun. 2002.

[3] R. J. Webster, "Mechanics of precurved-tube continuum robots," *IEEE Trans. Robot.*, vol. 25, no. 1, pp. 263–273, Feb. 2009.

[4] M. Grissom, V. Chitrakaran, D. Dienno, M. Csencsits, M. Pritts, B. Jones, W. McMahan, D. M. Dawson, C. Rahn, and I. D. Walker, "Design and experimental testing of the octarm soft robot manipulator," in *Proc. SPIE*, Orlando, FL, 2006.

[5] A. Degani, H. Choset, B. Zubiate, T. Ota, and M. Zenati, "Highly articulated robotic probe for minimally invasive surgery," in *Proc. Int. IEEE EMBS Conf.*, Vancouver, BC, Canada, 2008, pp. 3273–3276.

[6] M. W. Hannan and I. D. Walker, "A novel 'elephant's trunk' robot," in *Proc. 2000 IEEE/RSF Int. Conf. Intell. Robot. Syst.*, Takamatsu, Japan, 2000.

[7] H. B. Brown, M. Schwerin, E. Shammas, and H. Choset, "Design and control of a second-generation hyper-redundant mechanism," in *Proc. IEEE/RSJ Int. Conf. Intell. Robot. Syst.*, San Diego, CA, USA, 2007.

[8] I. A. Gravagne, C. D. Rahn, and I. D. Walker, "Large deflection dynamics and control for planar continuum robot," *IEEE/ASME Trans. Mechatron.*, vol. 8, no. 2, pp. 299–307, Jun. 2003.

[9] C. Thompson, M. Ryou, N. Soper, E. Hungess, R. Rothstein, and L. Swanstrom, "Evaluation of a manually driven, multitasking platform for complex endoluminal and natural orifice transluminal endoscopic surgery applications," *Gastrointest. Endos.*, vol. 70, no. 1, pp. 121–125, Jul. 2009.

[10] G. Dogangil, B. L. Davies, and F. R. Baena, "A review of medical robotics for minimally invasive soft tissue surgery," *Proc. Inst. Mech. Eng., Part H, J. Eng. Med.*, vol. 224, no. 653, pp. 653–679, 2010.

[11] B. W. Miedema, J. A. Astudillo, E. Sporn, and K. Thaler, "NOTES Techniques: Present and future," *Eur. Surg.*, vol. 40/3, pp. 103–110, 2008.

[12] S. Shaikh and C. Thompson, "Natural orifice translumenal surgery: Flexible platform review," *World J. Gastrointest. Surg.*, vol. 2, no. 6, pp. 210–216, Jun. 2010.

[13] A. Loeve, P. Breedveld, and J. Dankelman, "Scopes too flexible . . . and too stiff," *IEEE PULSE*, vol. 1, no. 3, pp. 26–41, Nov./Dec. 2010.

[14] Y. Chen, J. H. Chang, A. S. Greenlee, K. C. Cheung, A. H. Slocum, and R. Gupta, "Multi-turn, tension-stiffening catheter navigation system," in *Proc. IEEE Int. Conf. Robot. Autom.*, Anchorage, AK, USA, 2010.

[15] A. Petterssona, S. Davisb, J. O. Graybb, T. Doddc, and T. Ohlsson, "Design of a magnetorheological robot gripper for handling of delicate food products with varying shapes," *J. Food Eng.*, vol. 98, no. 3, pp. 332–338, Jun. 2010.

[16] J. Chen and W. Liao, "Design and control of a magnetorheological actuator for leg exoskeleton," in *Proc. IEEE Int.. Conf. Robot. Biomimetics*, Sanya, China, 2007, pp. 1388–1393.

[17] N. Cheng, G. Ishigami, S. Hawthorne, C. Hao, M. Hansen, M. Telleria, R. Playter, and K. Iagnemma, "Design and analysis of a soft mobile robot composed of multiple thermally activated joints driven by a single actuator," in *Proc. IEEE Int. Conf. Robot. Autom.*, Anchorage, AK, USA, 2010, pp. 5207–5212.

[18] M. Telleria, M. Hansen, D. Campbell, A. Servi, and M. Culpepper, "Modeling and implementation of solder-activated joints for single-actuator, centimeter-scale robotic mechanisms," in *Proc. IEEE Int. Conf. Robot. Autom.*, Anchorage, AK, USA, 2010, pp. 1681–1686.

[19] E. Brown, N. Rodenberg, J Amend, A. Mozeika, E. Steltz, M. Zakin, H. Lipson, and H. Jaeger, "Universal robotic gripper based on the jamming of granular material," in *Proc. Nat. Academy Sci. USA*, 2010, vol. 107.

[20] N. Cheng, M. Lobovsky, S. Keating, A. Setapen, K. Gero, A. Hosoi, and K. Iagnemma, "Design and analysis of a robust, low-cost, highly articulated manipulator enabled by jamming of granular media," in *Proc. IEEE/RSJ Int. Conf. Intell. Robot. Syst.*, 2012.

[21] Y. J. Kim, S. Cheng, S. Kim, and K. Iagnemma, "Design of a tubular snake-like manipulator with stiffening capability by layer jamming," in *Proc. IEEE/RSJ Int. Conf. Intell. Robot. Syst.*, 2012.

[22] Y. J. Kim, S. Cheng, S. Kim, and K. Iagnemma, "A novel layer jamming mechanism with tunable stiffness capability for minimally invasive surgery," *IEEE Trans. Robot. Autom.*, to be published.

Yong-Jae Kim received the M.S. and Ph.D. degrees in electrical engineering and computer science from the Korea Advanced Institute of Science and Technology, Daejeon, Korea, in 1998 and 2003, respectively.

He was a Principal Engineer with the Manufacturing Technology Center of Samsung Electronics, Kyunggi do, Korea. He is currently a Research Staff Member with the Samsung Advanced Institute of Technology, Kyunggi do, Korea. His research interests include the electromechanical design and control of hyper-redundant robots and humanoid robots and physical human–machine interaction.

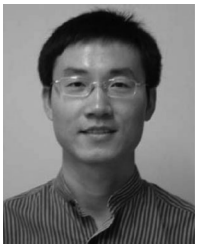

Shanbao Cheng received the B.S. and M.S. degrees from Sichuan University, Sichuan, China, and the Ph.D. degree from Nanyang Technological University, Singapore.

He is a senior R&D engineer with Ellipse Technologies, Irvine, CA, USA. In 2011, he was a Postdoctoral Researcher with the Massachusetts Institute of Technology, Cambridge, MA, USA, researching minimally invasive surgical robotics with variable stiffness. From 2008 to 2011, he was a Postdoctoral Researcher with the Rochester Institute of Technology, Rochester, NY, USA, developing magnetically levitated blood pumps. His research interests include mechatronics, magnetic bearings, artificial heart pumps, and rotor-dynamics analysis.

Sangbae Kim received the B.S. degree from Yonsei University, Seoul, Korea, in 2001 and the M.S. and Ph.D. degrees from Stanford University, Stanford, CA, USA, in 2004 and 2008, respectively, all in mechanical engineering.

He is the Director of the Biomimetic Robotics Laboratory and an Assistant Professor of mechanical engineering with the Massachusetts Institute of Technology (MIT), Cambridge, MA, USA. He is involved in the convergence of mechanical engineering, control, biology, and material science. He is currently focusing on the cheetah inspired robotic platform, which is capable of high-speed gallop, employing principles from quadrupedal runners. His achievement on bioinspired technology development includes the world's first directional adhesive based on gecko lizards and a climbing robot, i.e., Stickybot, that utilizes directional adhesives to climb smooth surfaces. Stickybot was featured as one of the best inventions of 2006 by *TIME Magazine*, and a paper on Stickybot won the best paper award for the IEEE TRANSACTIONS ON ROBOTICS in 2008 and for the IEEE International Conference on Robotics and Automation in 2007. His research interest includes design process extracting principles from complex biological systems to achieve legged locomotion in engineering.

Karl Iagnemma received the B.S. degree from the University of Michigan, Ann Arbor, MI, USA, and the M.S. and Ph.D. degrees from The Massachusetts Institute of Technology (MIT), Cambridge, MA, USA.

He is a Principal Research Scientist with MIT and the Director of the Robotic Mobility Group, where he was a National Science Foundation Graduate Fellow. He is author of the monograph *Mobile Robots in Rough Terrain: Estimation, Planning and Control with Application to Planetary Rovers* (Springer, 2004). He has recently led research programs for organizations including the U.S. Army Tank-Automotive and Armaments Command, the Army Research Office, DARPA, the NASA Mars Program Office, Ford Motor Company, Nissan, and Samsung, among others. He has authored or coauthored nearly 100 conference and journal papers on a wide range of robotic topics. His primary research interests include the design, sensing, motion planning, and control of mobile robots in challenging environments.

Dr. Iagnemma has served as an Associate Editor of the IEEE TRANSACTIONS ON ROBOTICS and the *Journal of Field Robotics* and has been the Co-editor of books on the DARPA Grand Challenge and Urban Challenge Autonomous Vehicle competitions.